Erschienen in: Dalton Transactions ; 44 (2015), 12. - S. 5510-5519
https://dx.doi.org/10.1039/C4DT03606A

Dalton Transactions

PAPER

View Article Online
View Journal | View Issue

Cite this: *Dalton Trans.*, 2015, **44**, 5510

The role of molecular oxygen in the iron(III)-promoted oxidative dehydrogenation of amines

Juan Pablo Saucedo-Vázquez,[a] Peter M. H. Kroneck[b] and Martha Elena Sosa-Torres*[a]

A mechanistic study is presented of the oxidative dehydrogenation of the iron(III) complex $[Fe^{III}L^{3}]^{3+}$, **1**, (L^3 = 1,9-bis(2′-pyridyl)-5-[(ethoxy-2″-pyridyl)methyl]-2,5,8-triazanonane) in ethanol in the presence of molecular oxygen. The product of the reaction was identified by NMR spectroscopy and X-ray crystallography as the identical monoimine complex $[Fe^{II}L^{4}]^{2+}$, **2**, (L^4 = 1,9-bis(2′-pyridyl)-5-[(ethoxy-2″-pyridyl)-methyl]-2,5,8-triazanon-1-ene) also formed under an inert nitrogen atmosphere. Molecular oxygen is an active player in the oxidative dehydrogenation of iron(III) complex **1**. Reduced oxygen species, *e.g.*, superoxide, ($O_2^{\bullet-}$) and peroxide (O_2^{2-}), are formed and undergo single electron transfer reactions with ligand-based radical intermediates. The experimental rate law can be described by the third order rate equation, $-d[(Fe^{III}L^{3})^{3+}]/dt = k_{OD}[(Fe^{III}L^{3})^{3+}][EtO^-][O_2]$, with k_{OD} = 3.80 ± 0.09 × 10^7 M^{-2} s^{-1} (60 °C, μ = 0.01 M). The reduction $O_2 \rightarrow O_2^{\bullet-}$ represents the rate determining step, with superoxide becoming further reduced to peroxide as shown by a coupled heme catalase assay. In an independent study, with H_2O_2, replacing O_2 as the oxidant, the experimental rate law depended on $[H_2O_2]$: $-d[(Fe^{III}L^{3})^{3+}]/dt = k_{H_2O_2}[(Fe^{III}L^{3})^{3+}][H_2O_2]$), with $k_{H_2O_2}$ = 6.25 ± 0.02 × 10^{-3} M^{-1} s^{-1}. In contrast to the reaction performed under N_2, no kinetic isotope effect (KIE) or general base catalysis was found for the reaction of iron(III) complex **1** with O_2. Under N_2, two consecutive one-electron oxidation steps of the ligand coupled to proton removal produced the iron(II)-monoimine complex $[Fe^{II}L^{4}]^{2+}$ and the iron(II)-amine complex $[Fe^{II}L^{3}]^{2+}$ in a 1 : 1 ratio (disproportionation), with the amine deprotonation being the rate determining step. Notably, the reaction is almost one order of magnitude faster in the presence of O_2, with k_{EtO^-} = 3.02 ± 0.09 × 10^5 M^{-1} s^{-1} (O_2) compared to k_{EtO^-} = 4.92 ± 0.01 × 10^4 M^{-1} s^{-1} (N_2), documenting the role of molecular oxygen in the dehydrogenation reaction.

Received 25th November 2014,
Accepted 2nd February 2015

DOI: 10.1039/c4dt03606a

www.rsc.org/dalton

Introduction

The transition metal-promoted oxidative dehydrogenation of organic substrates, *e.g.*, amines and alcohols, has been studied extensively in chemical and biological systems both in the absence (anoxic conditions) and presence (oxic conditions) of dioxygen.[1] The ability to selectively transform organic and biological substrates by removing electrons, and/or adding oxygen atoms, is pervasive in biology[2] and critical to industrial applications.[3] High-resolution X-ray structures have been reported for numerous enzymes, yet their mechanism of action including the activation of molecular oxygen has still not been fully understood in many cases. Thus, further experimental and computational investigations will be needed.[4] Notably, synthetic metal complexes can perform these types of oxidative dehydrogenation reactions.[5a] For example, during the reaction of Fe^{III} with a macrocyclic ligand in methanol, under oxic conditions, a 1,3-diazacyclopentane ring moiety was formed. Obviously, methanol had been oxidized to formaldehyde, which then reacted with an uncoordinated ethylenediamine motif of the macrocyclic ligand.[5b] A similar oxidation reaction was reported for the tris(2-pyridylmethyl)amine-Fe^{III} complex, with formaldehyde acting as a bridge for the (μ-oxo)diiron^{III} unit.[5c] More recently, kinetic and structural data were presented for the iron-promoted dehydrogenation of a polyamine ligand under anoxic conditions, and spectroscopic and electrochemical studies helped to identify reaction intermediates and the final Fe^{II}-monoimine product[6a,b] (Fig. 1). Oxidative dehydrogenation reactions have been carried out in the presence of molecular oxygen, or other oxidants,[7] such as $[Fe^{III}(CN)_6]^{3-}$, $S_2O_8^{2-}$, or H_2O_2. Amongst those, O_2 appeared to be the most effective agent. Goedken and Busch, who investigated the dehydrogenation of tetra-azamacrocyclic ligands coordinated to Fe^{II} under oxic conditions, were able to isolate a Fe^{III} intermediate in acetonitrile, and they postulated an intramolecular

[a]*Departamento de Química Inorgánica y Nuclear, Facultad de Química, Universidad Nacional Autónoma de México, Ciudad Universitaria, México, D.F. 04510, México. E-mail: mest@unam.mx*
[b]*Fachbereich Biologie, Universität Konstanz, 78457 Konstanz, Germany*

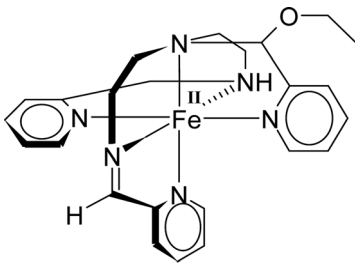

$[Fe^{II}L^4]^{2+}$

Fig. 1 Structure of the Fe(II)-imine complex **2**: $[Fe^{II}L^4]^{2+}$.

redox reaction *via* a ligand radical mechanism. However, the role of O_2 in the reaction was not elucidated.[7a] A recent study on the dehydrogenation of a N,O bidentate ligand led to an interesting application. Herein, the Cu^{II}-promoted formation of a fluorescent Cu^{I}–Schiff base complex allowed the selective detection of Cu^{II}. It was suggested that, as observed for related amine-containing ligands, the Cu^{I}–Schiff base complex was produced *via* the oxidative dehydrogenation of the two coordinated amine moieties by Cu^{II} and O_2.[8a,b]

Other examples of the oxidative dehydrogenation of amines in the presence of gold,[9] or $Ru_2(OAc)_4Cl$,[10] were reported most recently, with O_2 as a fundamental reagent to promote the conversion of an amine to its corresponding imine. In the case of gold nanoparticles, spectroscopic evidence was presented for the formation of a charge-transfer complex in odd-sized Au_nO_2 (n = 7, 9, 11, 21) systems, resulting in the formation of a superoxo ($O_2^{\bullet-}$) species bound to a formally cationic gold cluster.[11] Mechanistic investigations of the oxidation of ethanol and glycerol to acids over supported gold and platinum catalysts, with $^{18}O_2$ and $H_2{}^{18}O$, demonstrated that oxygen atoms originated from hydroxide ions instead of O_2 and were incorporated into the alcohol during the oxidation reaction. DFT calculations suggested that the reaction path involves both solution-mediated and metal-catalyzed elementary steps. Molecular oxygen was proposed to participate in the catalytic cycle not by dissociation to atomic oxygen but by regenerating hydroxide ions formed *via* the catalytic decomposition of a peroxide intermediate.[12] Clearly, the activation of O_2 at metal sites has been, and still is, a process of central interest both in chemistry and biology, especially with regard to the nature of the individual electron- and proton-transfer steps.[13] Electron transfer from metal centers, or from organic functional groups, can proceed *via* an inner- or an outer-sphere mechanism. Proton transfer can occur after the transfer of electrons, or concomitantly in a concerted proton-electron transfer or hydrogen-atom transfer reaction.[14] In the case of iron pentadentate N_5 and tetradentate N_4 complexes, it was firmly established that O_2 activation proceeded *via* an inner sphere mechanism. Thereby, high valent iron-oxo intermediates became stabilized as Fe^{IV} complexes carrying the Fe^{IV}=O unit.[15] Additionally, other systems were reported which followed an outer sphere electron transfer mechanism, such as the reduction of O_2 to H_2O_2 by a series of Ru^{II} ammine complexes in aqueous acidic solution (Table 1).[16] The Cu^{II} tetrakis(cyclohexyl)porphyrinogen complex was spontaneously oxidized by O_2 to the corresponding Cu^{III} species, producing one equivalent of superoxide anion, $O_2^{\bullet-}$. Steric crowding of the peripheral hydrogens of the starting material prevented any direct Cu–O_2 bond, and an outer sphere electron transfer reaction was proposed.[17] More recently, the use of O_2 in oxidations catalyzed by polyoxometalates has been reported, which often occurs *via* an outer-sphere mechanism.[18] In the case of the reduction of O_2 by structural Fe^{II} in naturally occurring silicate minerals, the activation of O_2 proceeded *via* an outer-sphere mechanism.[19] Similarly, replacing the catalytic Zn^{II} ion of horse liver alcohol dehydrogenase by Fe^{II}, oxidation experiments followed by Mössbauer spectroscopy showed that the spin-coupled system is an outer-sphere $Fe^{II}\cdots(O_2^{\bullet-})_{aq}$ complex occurring as an intermediate during iron(II)-catalyzed dioxygen activation.[20] The intradiol-cleaving catechol dioxygenases represent an interesting class of non-heme iron enzymes interacting with dioxygen. They harbour a mononuclear $[Fe^{III}\text{-}(His)_2(Tyr)_2]$ active site and cleave the carbon–carbon bond of the enediol moiety. The metal retains its iron(III) character throughout the catalytic cycle and activates the substrate for direct interaction with O_2, by introducing a radical character to the bound catecholate. The substrate becomes susceptible to O_2 attack, generating a transient alkylperoxo-Fe^{III} intermediate.[21]

Table 1 Reduction of O_2 by transition metal complexes[a]

Complex	k_{O_2} (M^{-1} s^{-1})	Ref.
$[Fe^{III}L^3]^{3+}$	9.14×10^{-2}	This work
$[Ru^{III}L^3]^{3+}$	3.25×10^{-2}	6e
$[Cr^{II}(5\text{-Cl-phen})_3]^{2+}$	2.5×10^{5}	36
$[Cr^{II}(bpy)_3]^{2+}$	6.0×10^{5}	36
$[Cr^{II}(phen)_3]^{2+}$	1.5×10^{6}	36
$[Cr^{II}(5\text{-Mephen})_3]^{2+}$	2.2×10^{6}	36
$[Cr^{II}(4\text{-}4'\text{-Me2bpy})_3]^{2+}$	1.4×10^{7}	36
$[Cr^{II}(4\text{-}7\text{-Me2bpy})_3]^{2+}$	2.5×10^{7}	36
$[Ru^{II}(NH_3)_6]^{2+}$	2.3×10^{1}	16
$[Ru^{II}(NH_3)_4(phen)]^{2+}$	7.7×10^{-3}	16
$[Ru^{II}(NH_3)_5(isn)]^{2+}$	1.1×10^{-1}	16
$[Ru^{II}(NH_3)_5(4\text{-vinyl-py})]^{2+}$	5.7×10^{-1}	16
$[Ru^{II}(en)_3]^{2+}$	3.6×10^{1}	16
$[Co^{II}(sep)_3]^{2+}$	4.3×10^{1}	38

[a] L^3 = 1,9-bis(2′-pyridyl)-5-[(ethoxy-2″-pyridyl)methyl]-2,5,8-triazanonane; bpy = bipyridine; en = ethylenediamine; Isn = isonicotinamide; phen = o-phenanthroline; py = pyridine; sep = sepulchrate, 1,3,6,8,10,13,16,19-octaazabicyclo[6.6.6]eicosane

Here we report on the oxidative dehydrogenation of an iron(III) complex in the presence of O_2. The hexadentate N_6 complex **1**, $[Fe^{III}L^3]^{3+}$ (L^3 = 1,9-bis(2′-pyridyl)-5-[(ethoxy-2″-pyridyl)methyl]-2,5,8-triazanonane) is converted to the Fe(II)-monoimine complex **2**, $[Fe^{II}L^4]^{2+}$ (L^4 = 1,9-bis(2′-pyridyl)-5-[(ethoxy-2″-pyridyl)methyl]-2,5,8-triazanon-1-ene). O_2 actively participates in the dehydrogenation of Fe(III) complex **1**. Reduced oxygen species, *e.g.*, superoxide, ($O_2^{\bullet-}$) and peroxide (O_2^{2-}), shown by a coupled enzymatic assay with catalase are formed, which undergo single electron transfer reactions

with ligand-based Fe(II)-radical intermediates. The experimental rate law can be described by a third order rate equation; the transfer of the first electron to O_2 yielding $O_2^{\bullet-}$ represents the rate determining step.

Experimental section

Materials

All chemicals were commercially available and used without further purification unless indicated. Both 5- and 6-carboxy-2′,7′-dichlorodihydrofluorescein diacetate (carboxy-H_2DCFDA) were purchased from Invitrogen; ethanol was carefully dried by distillation over magnesium, and kept under N_2, applying standard Schlenk techniques. Molecular oxygen (grade 5.0, Praxair) was used throughout. Hydrogen peroxide (30% in water) and potassium superoxide were from Aldrich, and Spin traps 5-*tert*-butoxycarbonyl 5-methyl-1-pyrroline *N*-oxide (BMPO) and 5,5-dimethyl-1-pyrroline *N*-oxide (DMPO) from Alexys Chemicals. Cu,Zn superoxide dismutase (SOD, bovine liver, Sigma-Aldrich, 70% Biuret) and heme catalase (CAT, *Neurospora crassa*) were a generous gift of Dr W. Hansberg Torres, Instituto de Fisiología, UNAM.

Syntheses. Ligand structures are depicted in Scheme 1; synthesis and characterization of 1-[3-aza-4-(2′-pyridyl)butyl]-2-(2″-pyridyl)-3-[(2‴-pyridyl)-methyl]imidazolidine (L^2) and $[Fe(DMSO)_6](NO_3)_3$ have been reported elsewhere.[6b,22] $[Fe^{II}L^4][BPh_4]_2$, (1,9-bis(2′-pyridyl)-5-[(ethoxy-2″- pyridyl methyl]-2,5,8-triazanon-1-ene)-iron(II) tetraphenylborate, complex **2**, was synthesized under O_2 which doubled the yield compared to the procedure under N_2.[6a] To a 50 mL solution of L^2 (1.01 mmol) in ethanol (60 °C, 10 psi O_2), $[Fe(DMSO)_6](NO_3)_3$ (720 mg, 1.01 mmol) was added in small portions, over a period of 1.5 h; the resulting purple solution was then stirred for another 4 h. To the cold solution, 5 mL of 0.5 M sodium tetraphenylborate in ethanol was added. The reaction mixture was kept at +4 °C for 30 min, and the resulting purple crystalline solid was recovered by filtration, washed with cold ethanol and dichloromethane, and finally dried under vacuum, giving 772 mg of **2** (69% yield). $C_{72}H_{70}B_2FeN_6O$: found C, 77.44; H, 6.16; N, 7.86%, calculated C, 77.71; H, 6.34; N, 7.55%; ^{1}HNMR and ^{13}CNMR spectra in acetone-d_6, recorded at 400 MHz at 298 K, showed the important features of complex **2**,[6a,b]: (i) the imine function at δ = 9.6 and 169.8 ppm, (ii) the hemi-aminal function (asymmetric carbon) at δ = 5.4 and 98.6 ppm. This carbon atom has an asymmetric center, thus, the neighbouring methylene groups become diastereotopic, giving resonances at δ = 3.96 and 4.09 ppm (^{1}H) and one for carbon at δ = 69.2 ppm (^{13}C).

Instrumentation and methods

Fourier transform infrared spectra (4000–200 cm^{-1}, KBr) were obtained on a Perkin-Elmer 599-B instrument; electronic absorption spectra (190–820 nm) were recorded on an Agilent 8453 diode array spectrophotometer. Luminescent experiments were carried out with a Perkin Elmer LS 50 Fluorescence Spectrometer. ^{1}H and ^{13}C NMR spectra were measured in acetone-d_6 on a Varian NMR Unity Plus-400 and 300 NMR Unity-Inova spectrometer, with TMS as an internal standard. EPR spectra were recorded under non-saturating conditions of microwave power on a Bruker Elexys E500 instrument at ≈9.40 GHz (X-band) and 100 kHz modulation frequency; spectra were evaluated with the Bruker software. The temperature was maintained with an Oxford liquid helium flow cryostat

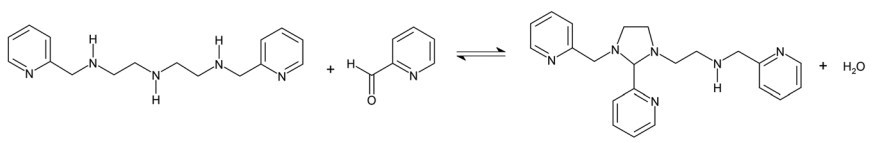

L^1 L^2

L^1 = 1,9-bis(2'-pyridyl)-2,5,8-triazanonane

L^2 = 1-[3-aza-4-(2'-pyridyl)butyl]-2-(2''-pyridyl)-3-[(2'''-pyridyl)-methyl]imidazolidine

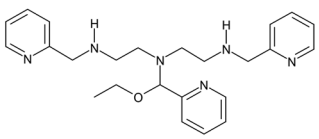

L^3 =1,9-bis(2'-pyridyl)-5-[(ethoxy-2''-pyridyl)methyl]-2,5,8-triazanonane

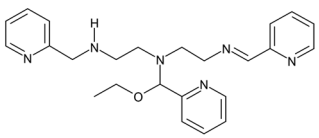

L^4 = 1,9-bis(2'-pyridyl)-5-[(ethoxy-2''-pyridyl)methyl]-2,5,8-triazanon-1-ene

Scheme 1 Ligands.

(10–20 K), or with a nitrogen flow system (110–300 K). The crystal structure of complex **2** was obtained with an Oxford Diffraction Gemini "A" instrument equipped with a CCD area detector ($\lambda_{MoK\alpha}$ = 0.71073 Å) and a sealed tube X-ray source at 100 K. Elemental analyses of C, H, N were carried out with a Fisons Instrument EA 1108.

Determination of pH* in ethanol. An Orion 720A pH meter, equipped with a combined glass electrode, was used to determine the pH* in ethanol at different temperatures; the reference electrode was Ag–AgCl in saturated LiCl–ethanol.[23] The system was calibrated against two standards[24] in ethanol, at 25 °C; standard 1, pH* = 5.02, [HCl] = 2.55 mmol kg^{-1}, [NaCl] = 10.19 mmol kg^{-1}; standard 2, pH* = 9.95, [acetic acid] = 25.5 mmol kg^{-1}, [sodium acetate] = 12.75 mol kg^{-1}, [NaCl] = 6.38 mmol kg^{-1}.

Preparation of buffers in ethanol. Buffers were prepared as described,[6a] by dissolving 2,4,6-trimethylpyridine in ethanol and addition of the appropriate amount of HCl until the desired pH* had been reached (determination of its pK_a in ethanol gave the value: 9.48 ± 0.05). The buffer capacity, pH* = pK_a ± 1, was determined by titrating a 0.5 M 2,4,6-trimethylpyridine buffer solution both with HCl and LiOH standard solutions; [EtO^-] was calculated according to [EtO^-] = $10^{-(19.1-pH^*)}$, the ionic product of EtOH was obtained from the literature,[25] and the ionic strength μ was maintained at 0.01 M with NaCl.

Concentration of molecular oxygen. Initial concentrations of dioxygen, $[O_2]_0$, in ethanol were determined with an YSI 5100 oximeter equipped with a gold cathode and a silver anode, set at a constant potential: −0.80 V/Ag–AgCl.

Electrochemical measurements. Data were obtained on an EG&G PAR Potentiostat-Galvanostat model 273-A, equipped with a three-electrode system, in ethanol containing 0.10 M LiCl as the supporting electrolyte; measurements were carried out using a double platinum electrode and a Ag^0–AgCl as the reference electrode. Potentials are reported *vs.* the ferrocene–ferrocenium redox couple, $Fc^{+/0}$: ΔE = 0.72 V.

Kinetic measurements. The reactions in ethanol, at constant pH*, were followed spectrophotometrically in a thermostatted 3.0 cm^3 cell, at 60 ± 0.1 °C; the ionic strength μ was kept constant at 0.01 M by adding the appropriate amount of NaCl. Spectra were recorded over the range 190–820 nm, and the rate constants were determined from the change in absorbance with time. Plots of $\ln|A_t - A_\infty|$ *vs.* time were linear; A_t and A_∞ represent the absorbance at time t and at the end of the reaction, respectively; A_∞ was determined after 10 half-lives. $[O_2]_0$ varied from 1.56×10^{-5} to 9.37×10^{-4} M, both [L^2] and [$Fe(DMSO)_6(NO_3)_3$] were 10^{-4} M. The overall process consisted of two reactions. First, the starting $[Fe^{III}L^3]^{3+}$ complex, **1**, was formed in a rapid reaction, by mixing solutions of L^2 and $Fe(DMSO)_6(NO_3)_3$ in ethanol. The reaction was followed at 344 nm over the pH* range 8.57–9.89, at 60 ± 0.1 °C, under different initial concentrations of O_2. The following oxidative dehydrogenation reaction started once **1** was formed. It was followed at 398 nm and led to the formation of the Fe(II)-monoimine complex **2**, under these experimental conditions. The second-order rate constants were calculated taking into account the K_{EtOH} at this temperature.[25]

Enzymatic assays

The presence of potential oxygen intermediates formed during the dehydrogenation reaction was investigated by using either SOD or CAT in independent experiments.

Catalase. The activity of CAT was determined at 27 °C in water–ethanol (80 : 20% v/v). 10 μL of 20 mg mL^{-1} CAT in 0.10 M K+ phosphate buffer, pH = 8.0 were mixed with 3.0 mL water–ethanol, to which aliquots of 0.10 M H_2O_2 in aqueous solution, were added to give final H_2O_2 concentrations of 0.07, 0.2, 0.3, 0.4, 1.0, 2.0 and 5.0 mM. The concentration of H_2O_2 in the stock solution was determined as reported in the literature.[26]

Superoxide dismutase. The activity of SOD was determined at 27 °C in the water–ethanol mixture according to Fridovich.[27] Lyophilized SOD was dissolved in 0.10 M K^+ phosphate buffer, pH = 8.0; potassium superoxide, dissolved in THF, served as a source for superoxide. 10 μL of 20 mg mL^{-1} SOD in 0.10 M K^+ phosphate buffer, pH 8.0, was mixed with 3.0 mL water–ethanol, to which aliquots of 0.5 M KO_2 in tetrahydrofuran were added to give final superoxide concentrations of 0.01, 0.05 and 0.10 mM. The concentration of O_2, produced by either SOD ($2O_2^{\bullet-} + 2H^+ \rightarrow O_2 + H_2O_2$), or CAT ($2H_2O_2 \rightarrow O_2 + 2H_2O$), was monitored with the oximeter described above; a linear dependence of the corresponding enzyme activity was obtained under these experimental conditions (data not shown).

H_2DCFDA experiments. A 25 μM solution (40 μL) of the superoxide indicator carboxy-H_2DCFDA was added directly to the reaction and incubated for 20 min, hereafter the mixture was transferred to a 3 cm^3 quartz cell to determine the luminescence at 500 nm.[28]

Results and discussion

Previously we had reported on the oxidative dehydrogenation of iron(III) complex $[Fe^{III}L^3]^{3+}$ **1**, under the exclusion of molecular oxygen, with the iron(II)-monoimine complex $[Fe^{II}L^4]^{2+}$ **2**, as one final reaction product (Fig. 1). This complex was formed by disproportionation of the starting iron(III) complex **1** (eqn (1))

$$2[Fe^{III}L^3]^{3+} + 2EtO^- \rightarrow [Fe^{II}L^4]^{2+} + [Fe^{II}L^3]^{2+} + 2EtOH \quad (1)$$

via a three-step reaction mechanism, with ligand-centered radical intermediates. The rate law could be described by a second-order rate equation. General base catalysis and a primary kinetic isotope effect k_{EtOH}/k_{EtOD} of 1.73 were detected, and deprotonation of the coordinated amine became the rate determining step in the oxidative dehydrogenation reaction.[6a]

We now investigated the reaction of complex **1** in the presence of molecular oxygen. Overall, the formation of $[Fe^{III}L^3]^{3+}$ from L^2 and $Fe(DMSO)_6(NO_3)_3$ in ethanol is fast compared to the dehydrogenation reaction and does not depend on pH*

(range 8.57–9.89) nor on the concentration of O_2. Once the iron(III)-polyamine complex **1** has been formed, the actual oxidative dehydrogenation starts producing the purple iron(II)-monoimine complex **2**. The product is diamagnetic and has a well-resolved ^{1}H-NMR spectrum showing a chemical shift δ = 9.60 for the acidic proton of the imine moiety. In order to corroborate the structure of complex **2** produced under oxic conditions, crystals obtained in acetone were analyzed by X-ray diffraction. All angles and bond lengths were practically identical to those reported earlier for the structures of $\mathbf{2_r}$[6b] and $\mathbf{2_{Oh.}}$[6a]

Electrochemical studies

The participation of O_2 in the dehydrogenation reaction of complex **1** was documented by measuring its consumption with the oximeter (Fig. 2), and by cyclic voltammetry (Fig. 3). For the Fe^{III}/Fe^{II} pair of $[Fe(DMSO)_6]^{3+}$, $E_{1/2}$ = −0.542 V *vs.* $Fc^{+/0}$ was determined (Fig. 3d). At time zero, a 1 : 1 mixture of $[Fe(DMSO)_6](NO_3)_3$ and L^2 (0.02 M), and 0.94 mM $[O_2]_0$ gave a reversible signal at $E_{1/2}$ = −0.425 V *vs.* $Fc^{+/0}$ (Fig. 3a) which was assigned to the Fe^{III}/Fe^{II} couple of the iron(III)-amine complex $[FeL^3]^{3+}$, **1**. After approximately 1 h, two features at E_{AP} = 0.013 and 0.172 V *vs.* $Fc^{+/0}$ appeared (Fig. 3b). These values compared well with E_{AP} = 0.067 and 0.198 V *vs.* $Fc^{+/0}$ recorded for the isolated iron(II)-monoimine complex $[FeL^4]^{2+}$ **2** (Fig. 3c). Furthermore, it became evident that (i) the reaction progressed faster under oxic conditions, and that (ii) only one product was formed, and not two as observed under N_2.[6a,b]

Stoichiometry and kinetics of the oxidative dehydrogenation of complex 1 in the presence of O_2

Two mechanistically different pathways have been observed under anoxic (N_2) and oxic (O_2) conditions. Under N_2, two consecutive one-electron oxidation steps coupled to proton removal from the amine ligand occurred, with ligand-centered radicals as intermediates in a disproportionation reaction (eqn (1)). Under oxic conditions, the participation of O_2 and reduced oxygen species as effective oxidants became crucial for electron transfer. The redox-states of the iron complexes formed in solution were unequivocally assigned by cyclic voltammetry, showing an intramolecular redox process between Fe^{III} and the coordinated amine ligand plus electron transfer to O_2, with the following overall stoichiometry (eqn (2)).

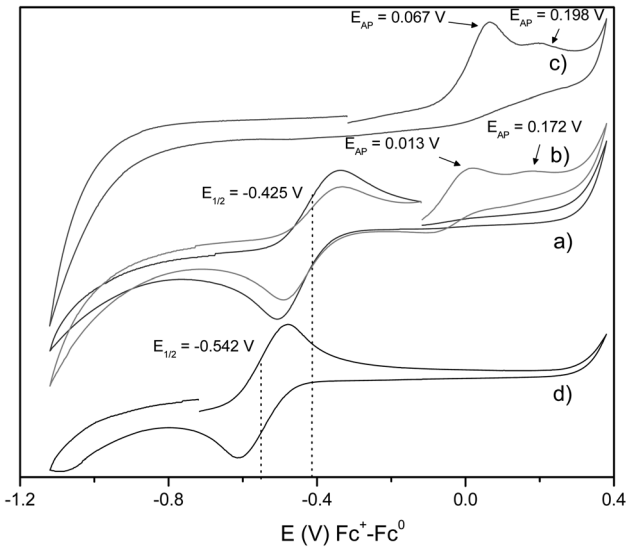

Fig. 3 Oxidative dehydrogenation of complex **1**, $[Fe^{III}L^3]^{3+}$, measured by cyclic voltammetry of a 1 : 1 mixture of 0.02 M $[Fe(DMSO)_6](NO_3)_3$ and L^2 and 0.94 mM $[O_2]_0$ in ethanol; supporting electrolyte 0.10 M LiCl, pH* = 9.89, recorded at different time intervals. (a) $t \approx 0$; (b) 1 h; (c) isolated final product, $[Fe^{II}L^4](BPh_4)_2$; (d) 0.02 M $[Fe(DMSO)_6](NO_3)_3$ in ethanol.

$$4[Fe^{III}L^3]^{3+} + O_2 + 4EtO^- \rightarrow 4[Fe^{II}L^4]^{2+} + 2H_2O + 4EtOH \quad (2)$$

The dehydrogenation of the coordinated amine ligand L^3 leads to monoimine ligand L^4. The insertion of the C=N double bond requires the release of two electron equivalents per amine ligand, which are used to reduce 4Fe(III) to 4Fe(II) and one molecule O_2 to two molecules H_2O. At acidic pH*, the oxidative dehydrogenation of complex **1** does not occur, whereas at neutral or basic pH*, formation of the iron(II)-monoimine complex **2** and $O_2^{\bullet-}$ is favored as outlined in Scheme 2.

The dehydrogenation reaction was followed by UV/vis spectroscopy over the time range of approximately 7 h, in a tightly sealed optical cell, at a defined initial $[O_2]_0$, pH* range 8.57–9.89, 60 ± 0.1 °C (Fig. 4A). It is started by mixing the imidazolidine ligand L^2 with $[Fe(DMSO)_6](NO_3)_3$ in ethanol in a 1 : 1 ratio. First, complex **1**, $[Fe^{III}L^3]^{3+}$ is formed with its characteristic absorption maxima at λ_1 = 582 (ε = 528 M^{-1} cm^{-1}) and at λ_2 = 366 nm (ε = 3390 M^{-1} cm^{-1}). The observed rate constant, k_{obs} for the formation of complex **1** in the presence of O_2 does not depend on pH* (Table 2) and is practically identical to k_{obs} obtained under N_2.[6a,e]

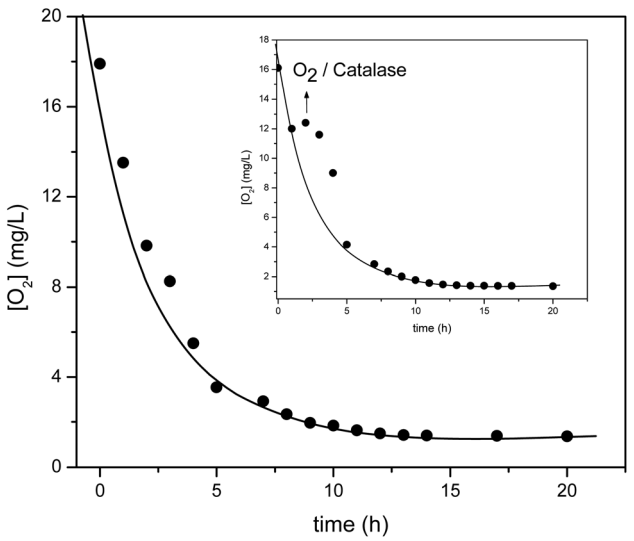

Fig. 2 Consumption of O_2 during the oxidative dehydrogenation of complex **1**, $[Fe^{III}L^3]^{3+}$, measured by oximetry in a 0.02 M $[Fe(DMSO)_6](NO_3)_3$ and 0.02 M L^2 reaction mixture in ethanol, pH* = 9.89. Insert: O_2 liberated during the dehydrogenation reaction in the presence of heme catalase, according to $2H_2O_2 \rightarrow O_2 + 2H_2O$.

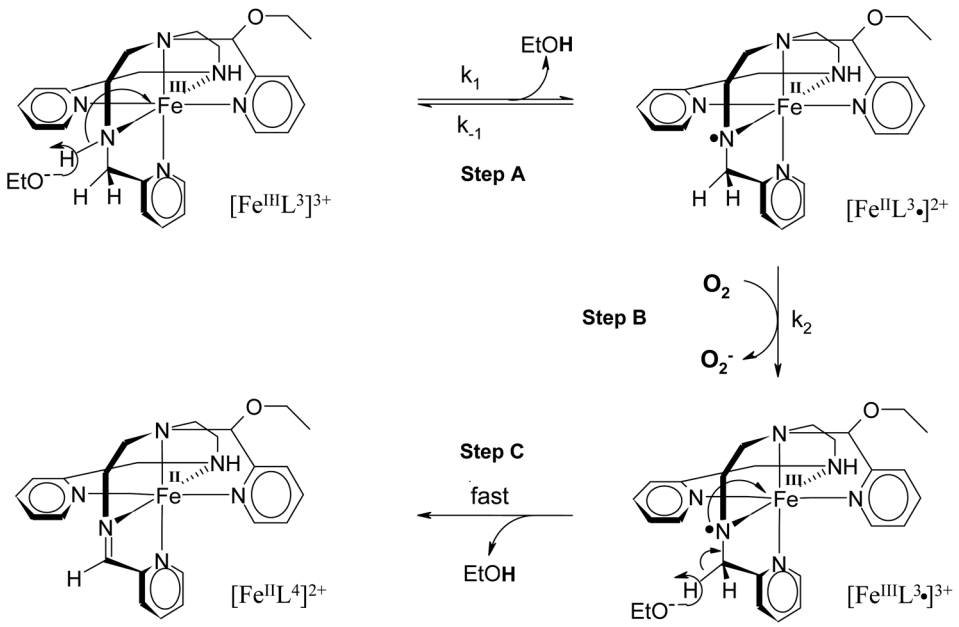

Scheme 2 Simplified mechanistic view of the oxidative dehydrogenation reaction of iron(III)-amine complex **1**, $[Fe^{III}L^3]^{3+}$, in the presence of molecular oxygen. Step (A) ligand deprotonation and formation of ligand-centered radical $[Fe^{II}L^{3\bullet}]^{2+}$. Step (B) formation of superoxide anion, $O_2^{\bullet-}$, leading to $[Fe^{III}L^{3\bullet}]^{3+}$. Step (C) ligand deprotonation and formation of final product, iron(II)-monoimine complex $[Fe^{II}L^4]^{2+}$; the formation of superoxide anion, $O_2^{\bullet-}$, represents the rate-determining step, k_2.

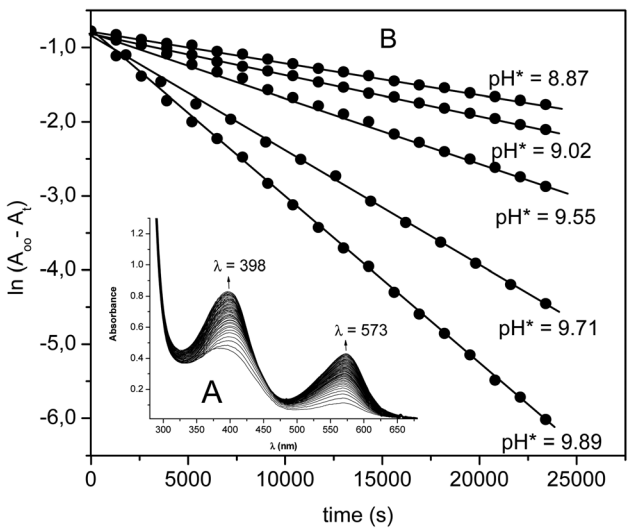

Fig. 4 (A) Oxidative dehydrogenation of complex **1**, $[Fe^{III}L^3]^{3+}$, followed by UV/vis spectroscopy of a 1 : 1 mixture of $[Fe(DMSO)_6](NO_3)_3$ and L^2 (0.02 M), and 0.94 mM $[O_2]_0$ in ethanol; pH* 9.89, 60 °C, spectra recorded at 30 min intervals; (B) dependence of k_{obs} on pH*, determined at 398 nm.

Table 2 Observed first order rate constant of the formation of complex **1**, $[Fe^{III}L^3]^{3+}$, 0.94 mM $[O_2]_0$, pH* 8.57–9.89, 60 °C, μ = 0.01 M

pH*	$10^5\ k_{obs}\ (s^{-1})$
8.57	3.23
9.02	3.17
9.55	3.09
9.89	3.25

The consecutive dehydrogenation process yields complex **2**, $[Fe^{II}L^4]^{2+}$, with its characteristic absorption maxima λ_1 = 573 nm (ε = 6984 M^{-1} cm^{-1}) and λ_2 = 398 nm (ε = 8036 M^{-1} cm^{-1}), and E_{AP} = 0.013 and 0.172 V *vs.* $Fc^{+/0}$ (Fig. 3b, 4A). The reaction does not proceed further once the iron(II)-monoimine complex **2** has been formed. The C=N double bond conjugated to the pyridine ring stabilizes the Fe^{II} oxidation state because of its π-acceptor capability, which is consistent with the high redox potential reported above.

Note that the yield of the iron(II)-monoimine complex **2** is 69% when prepared under oxic conditions, compared to 33% when prepared under anoxic conditions, showing that two different reaction mechanisms must be operative. The difference in yield reflects the different stoichiometries of the reaction when performed under N_2 or O_2 (eqn (1) and (2)). Under N_2,[6a,b] two iron(II) complexes are formed, $[Fe^{II}L^4]^{2+}$ (the Fe^{II}-monoimine complex **2**), and $[Fe^{II}L^3]^{2+}$ (the Fe^{II}-amine complex), whereas under O_2, solely the iron(II)-monoimine complex **2** is produced which explains the observed increase in yield.

Rate law and oxidative dehydrogenation reaction mechanism

The rate of the oxidative dehydrogenation of iron(III) complex **1** in the presence of O_2, showed a linear dependence of k_{obs} on pH* (Fig. 4B, Table 3). When the reaction was carried out at different concentrations of the base 2,4,6-trimethylpyridine, the reaction rate was not affected (data not shown), in contrast to the reaction performed under N_2.[6a]

Table 3 pH* dependence of the observed first-order and calculated second-order rate constants for the oxidative dehydrogenation of complex **1**, $[Fe^{III}L^3]^{3+}$, 0.94 mM $[O_2]_0$, 60 °C, μ = 0.01 M

pH*	10^{10} [EtO$^-$] (M)	10^5 k_{obs} (s^{-1})	10^{-5} k_{EtO^-} (M^{-1} s^{-1})
8.57	0.29	4.23	5.70
9.02	0.83	5.65	3.75
9.55	2.82	8.98	2.23
9.71	4.49	15.4	2.87
9.89	6.17	22.5	3.24

As the reaction rate depended on the initial concentration of O_2, $[O_2]_0$, a plot of k_{obs} against $[O_2]_0$ revealed a linear relationship (Fig. 5, Table 4), giving the second order rate constant, k_{O_2} = 9.14 ± 0.06 × 10^{-2} M^{-1} s^{-1}. Interestingly, the dehydrogenation of amine complex **1** to monoimine complex **2** was almost one order of magnitude faster under O_2, with k_{EtO^-} = 3.02 ± 0.09 × 10^5 M^{-1} s^{-1} (O_2) compared to k_{EtO^-} = 4.92 ± 0.01 × 10^4 M^{-1} s^{-1} (N_2), confirming the active role of O_2 in the reaction with the Fe(III) complex **1** (Fig. 6).

From the kinetic data, the following experimental third-order rate law is obtained (eqn (3)).

$$-\frac{d[(Fe^{III}L^3)^{3+}]}{dt} = k_{OD}[(Fe^{III}L^3)^{3+}][EtO^-][O_2] \quad (3)$$

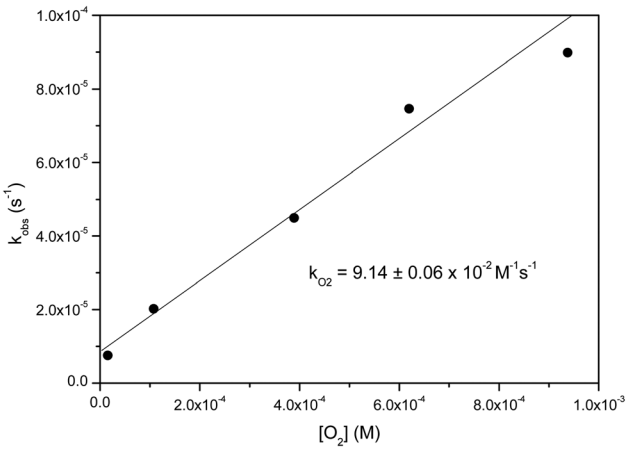

Fig. 5 Second order rate constant, k_{O_2}, obtained from the dependence of the first order rate constant, k_{obs}, on the initial $[O_2]_0$ concentration; 1.0 mM complex **1** in ethanol, pH* 9.55, 60 °C, μ = 0.01 M.

Table 4 $[O_2]_0$ dependence of the observed first-order rate constant k_{obs} and calculated second-order rate constant k_{O_2} for the oxidative dehydrogenation of complex **1**, $[Fe^{III}L^3]^{3+}$ in ethanol, pH* = 9.95, 60 °C, μ = 0.01 M

10^4 $[O_2]_0$ (M)	10^5 k_{obs} (s^{-1})	10^2 k_{O_2} (M^{-1} s^{-1})
0.15	0.76	13.7
1.08	2.04	9.96
3.89	4.49	9.07
6.20	7.48	10.5
9.37	8.98	8.55

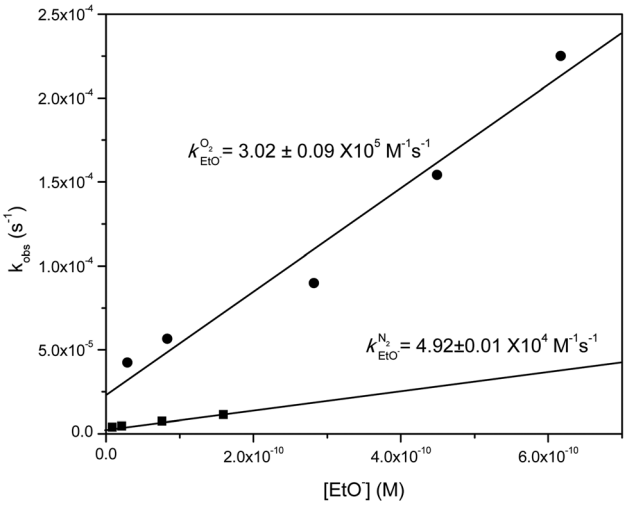

Fig. 6 Comparison of the rate constants k_{EtO^-} under O_2, and k_{EtO^-} under N_2 (taken from ref. 6a); both at 60 °C, μ = 0.01 M.

Based on these results, we propose the following mechanism:

$$4[Fe^{III}L^3]^{3+} + 4EtO^- \underset{k_{-1}}{\overset{k_1}{\rightleftharpoons}} 4[Fe^{II}L^3\bullet]^{2+} + 4EtOH \quad (4)$$

$$[Fe^{II}L^3\bullet]^{2+} + O_2 \xrightarrow{k_2} [Fe^{III}L^3\bullet]^{3+} + O_2^{\bullet-} \quad (5)$$

$$[Fe^{II}L^3\bullet]^{2+} + O_2^{\bullet-} \xrightarrow{k_3} [Fe^{III}L^3\bullet]^{3+} + O_2^{2-} \quad (6)$$

$$[Fe^{II}L^3\bullet]^{2+} + O_2^{2-} \xrightarrow{k_4} [Fe^{III}L^3\bullet]^{3+} + O^{\bullet-} + O^{2-} \quad (7)$$

$$[Fe^{II}L^3\bullet]^{2+} + O^{\bullet-} \xrightarrow{k_5} [Fe^{III}L^3\bullet]^{3+} + O^{2-} \quad (8)$$

$$4H^+ + 2O^{2-} \rightleftarrows 2H_2O \quad (9)$$

$$4[Fe^{III}L^3\bullet]^{3+} + 4EtO^- \xrightarrow{fast} 4[Fe^{II}L^4]^{2+} + 4EtOH \quad (10)$$

First, the coordinated amine ligand becomes deprotonated to the short-lived ligand-centered radical $[Fe^{II}L^3\bullet]^{2+}$ (eqn (4)), which reacts with O_2 to the second short-lived radical $[Fe^{III}L^3\bullet]^{3+}$ and the superoxide anion, $O_2^{\bullet-}$ (eqn (5)). In consecutive steps (eqn (6)–(8)) $[Fe^{II}L^3\bullet]^{2+}$ reacts with reduced oxygen species ($O_2^{\bullet-}$, O_2^{2-}, $O^{\bullet-}$) to produce $[Fe^{III}L^3\bullet]^{3+}$ and two molecules of H_2O. For reasons of simplicity we omitted the fast protonation steps of the oxygen species with the exception of O^{2-} (eqn (9)). $[Fe^{III}L^3\bullet]^{3+}$ is converted to the iron(II)-monoimine complex **2** as the final product (eqn (10)). Attempts to trap the $O_2^{\bullet-}$ anion, or one of the ligand-based radical complexes with DMPO or BMPO remained unsuccessful under the experimental conditions. The types of radicals described here are highly reactive.[6a] However, the electron deficiency on the ligand-based radical can be stabilized either by electron-donating groups or by coordination to a transition metal ion,[29] as shown for an aminyl radical-rhodium(I) complex.[30] Recently, single-electron transfer from a redox-active ligand to a bound substrate mediated by redox-inactive Pd(II) was reported, and a

ligand-based radical complex could be identified by EPR spectroscopy under anoxic conditions.[31]

Applying the steady-state approximation to the first radical intermediate, the treatment leads to the following rate law (eqn (11)):

$$-\frac{d[(Fe^{III}L^3)^{3+}]}{dt} = \frac{4k_1k_2[(Fe^{III}L^3)^{3+}][EtO^-][O_2]}{k_{-1} + k_2[O_2]} \quad (11)$$

In the limit $k_{-1} \gg k_2[O_2]$, expression (11) reduces to the third order rate law (eqn (12)), with the experimental third order constant, k_{OD}, related to the individual rate constants as outlined in eqn (13).

$$-\frac{d[(Fe^{III}L^3)^{3+}]}{dt} = \frac{4k_1k_2}{k_{-1}}[(Fe^{III}L^3)^{3+}][EtO^-][O_2] \quad (12)$$

$$k_{OD} = \frac{4k_1k_2}{k_{-1}} \quad (13)$$

Overall, the proposed reaction mechanism (eqn (4)–(10)) is consistent with the experimental rate law (eqn (3)). Under the experimental conditions, the reduction of O_2 to $O_2^{\bullet-}$ (eqn (5)), k_2, becomes rate determining, as expected in view of the finding that this process is thermodynamically unfavorable.[32] However, contrary to the reaction performed under N_2, no kinetic isotope effect (KIE) plus general base catalysis were found for the reaction of iron(III) complex **1** with O_2. It is reasonable to assume that the central Fe(III) activates the L^3 ligand in the region of the coordinated secondary nitrogen and the adjacent CH_2 moiety,[7a] facilitating the formation of ligand-based radical $[Fe^{II}L^{3\bullet}]^{2+}$ which then reacts with whatever external oxidizing agent is available, here with O_2 and reduced oxygen species (eqn (4)–(8); Scheme 2). A similar scenario was described for the intradiol-cleaving catechol dioxygenases and several structural and functional mimetic complexes thereof.[21] Once formed, the negatively charged oxygen species can interact directly with the iron(III) complex **1**, $[Fe^{III}L^3]^{3+}$, enhancing the rates of proton and electron transfer, which might explain the absence of a KIE. In this context, Fukuzumi and colleagues reported about the oxidative reactivity of the non-heme $[Fe^{IV}(O)(N_4Py)]^{2+}$ complex in acetonitrile which could be remarkably influenced, *e.g.*, by addition of Sc^{3+} or $HClO_4$. Depending on the experimental conditions, the KIE values drastically decreased accompanied by remarkably enhanced reaction rates.[33] For another class of non-heme iron enzymes, the lipoxygenases, it is generally believed that after the initial hydrogen atom abstraction by Fe(III), forming the substrate radical and Fe(II), the activated substrate becomes oxygenated to the corresponding alkylhydroperoxide product.[14,34] Recently, a new mechanism for O_2 activation in the presence of iron(III) was brought forward. Iron(III) interacted with the known charge-transfer complex formed between the substrate linoleic acid and O_2 leading to a ternary complex Fe^{III}–O_2-substrate, giving the substrate hydroperoxide product without change of the iron oxidation state.[35]

Further evidence for the active role of O_2 and formation of reduced oxygen species during the dehydrogenation reaction came from experiments with heme catalase (CAT). When fixed amounts of CAT were added to aliquots of the reaction mixture at different times, a distinct increase of dissolved O_2 could be detected, documenting the formation of hydrogen peroxide and its decomposition to O_2 and water (Fig. 2, insert). Attempts to detect free superoxide, $O_2^{\bullet-}$, during the course of the dehydrogenation reaction, using either carboxy-H_2DCFDA or SOD, remained unsuccessful, most probably due to its fast conversion to peroxide under the experimental conditions. Superoxide (KO_2, dissolved in DMF) and peroxide (H_2O_2, 30% in water) were also tested as oxidants in independent kinetic studies in ethanol, pH* 9.55. Superoxide did react, however, good reproducible kinetic data could not be obtained. Peroxide was also an active oxidant, in this case the experimental rate depended on $[H_2O_2]$: $-d[(Fe^{III}L^3)^{3+}]/dt = k_{H_2O_2}[(Fe^{III}L^3)^{3+}][H_2O_2]$, with $k_{H_2O_2} = 6.25 \pm 0.02 \times 10^{-3}$ M^{-1} s^{-1}. (Fig. 7, Table 5). The oxidative dehydrogenation was slow compared to the reaction with molecular oxygen. Most likely, water (≈3–30 mM in the kinetic assay) interferes with the principal reaction.[7a]

The experimental finding that peroxide is formed during the dehydrogenation of iron(III) complex **1**, suggests that the reaction proceeds *via* an outer sphere electron transfer mechanism. The second order rate constant, $k_{O_2} = 9.14 \pm 0.06 \times 10^{-2}$ M^{-1} s^{-1} obtained in this work is in the same range of magni-

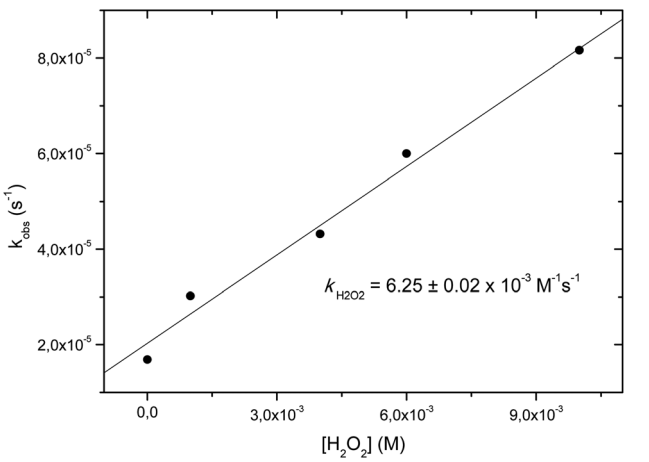

Fig. 7 Second order rate constant $k_{H_2O_2}$ obtained from the $[H_2O_2]_0$ dependence of the first order rate constant, k_{obs}, for the oxidative dehydrogenation of complex **1**, $[Fe^{III}L^3]^{3+}$, 0.10 mM in ethanol, pH* 9.55, 60 °C, μ = 0.01 M.

Table 5 $[H_2O_2]$ dependence of the observed first-order rate constant k_{obs} and the calculated second-order rate constant $k_{H_2O_2}$ for the oxidative dehydrogenation of complex **1**, $[Fe^{III}L^3]^{3+}$ in ethanol, pH* = 9.95, 60 °C, μ = 0.01 M

10^3 $[H_2O_2]$ (M)	10^5 k_{obs} (s^{-1})	10^3 $k_{H_2O_2}$ (M^{-1} s^{-1})
1.00	3.02	10.2
4.01	4.32	5.80
6.00	6.00	6.66
10.17	8.16	6.16

tude reported by Taube and coworkers for the reduction of O_2 to H_2O_2 with various Ru^{II}-ammine complexes (Table 1).[16] According to those authors the reduction of O_2 proceeded by a one-electron outer sphere transfer mechanism. Espenson and coworker observed a several orders of magnitude faster reduction of O_2 to $O_2^{\bullet-}$ (Table 1).[36] Again, an outer sphere electron transfer mechanism was assumed for the production of the superoxide anion. In the case of the iron(III) complex $[Fe^{III}L^3]^{3+}$ **1** forming the radical $[Fe^{II}L^{3\bullet}]^{2+}$, with the metal center surrounded by a bulky hexadentate nitrogen ligand, an inner sphere electron transfer mechanism between iron and O_2 appears not very likely, for similar reasons as brought forward for the Cu^{II}-tetrakis(cyclohexyl)porphyrinogen complex. In this case, steric crowding of the peripheral hydrogens prevented any direct Cu–O_2 bond, and an outer sphere electron transfer reaction was proposed.[17]

Conclusions

In a simplified scheme for O_2 activation by transition metals, we generally assume a metal site, *e.g.*, a mononuclear iron center in the reduced iron(II) oxidation state which binds to the O_2 molecule and reduces it to the superoxide adduct. The metal site can also be coordinated to "non-innocent" ligands capable of providing reducing equivalents. The Fe^{III}–superoxide adduct will be reduced further to the peroxide level, with concomitant delivery of a proton. Cleavage of the O–O bond will then occur to yield iron-oxo (or -oxyl species), again with possible involvement of additional protons. At each stage of the process, electrons flow to the coordinated O_2 moiety, either from the ligand unit or from an external source.[37] In the system described here, we start with the iron(III) complex **1**, $[Fe^{III}L^3]^{3+}$, with the hexadentate N_6 ligand 1,9-bis(2′-pyridyl)-5-[(ethoxy-2″-pyridyl)methyl]-2,5,8-triazanonane which undergoes an oxidative dehydrogenation (Scheme 2, steps A–C) in the presence of molecular oxygen in ethanol at basic pH*. The reaction proceeds *via* successive oxidation of the ligand-based radical intermediate $[Fe^{II}L^{3\bullet}]^{2+}$ (Scheme 2, step A), by O_2 and reduced oxygen species (*e.g.*, superoxide, peroxide; Scheme 2, step B) to yield the final product, the iron(II)-monoimine complex **2**, $[Fe^{II}L^4]^{2+}$ (Scheme 2, step C). One might envision the direct reaction between the starting iron(III) complex $[Fe^{III}L^3]^{3+}$ and O_2 followed by proton transfer (EtO^-) *via* a kind of a ternary complex, giving $[Fe^{III}L^{3\bullet}]^{3+}$, $O_2^{\bullet-}$ and H^+ (EtOH), in order to understand the lack of KIE. The radical $[Fe^{III}L^{3\bullet}]^{3+}$ would then react with EtO^- to the final product, the Fe(II)-monoimine complex **2**. However, this mechanism is not compatible with the experimental rate law (eqn (3)). The formation of $O_2^{\bullet-}$ becomes rate determining under oxic conditions whereas under anoxic conditions ligand deprotonation (primary kinetic isotope effect (k_{EtOH}/k_{EtOD}) = 1.73) followed by electron transfer was rate determining.[6a] The detection of O_2 liberated by CAT from H_2O_2 produced during the dehydrogenation reaction suggests that the reduction of O_2 by the Fe^{II}-radical intermediates proceeds *via* an outer sphere electron transfer mechanism, because of steric crowding as described for the Cu(II)-porphyrinogen complex.[17] At this point, the absence of a KIE for the oxidative dehydrogenation of $[Fe^{III}L^3]^{3+}$ under oxic conditions is not well understood. However, the recent studies of Fukuzumi and colleagues document in an impressive manner how reaction rates and KIEs can be dramatically influenced by rather simple changes of the experimental conditions.[33]

Additional experimental data are needed to extend and/or modify the proposed reaction mechanism to obtain better insight into the various factors that govern it. In view of the importance of the interaction of Fe(III) and O_2 in chemistry, biology and the environment, the results presented here will be of great value.

Acknowledgements

M.E.S.T. gratefully acknowledges the financial support by DGAPA-UNAM (Research project IN231111) and CONACYT (Research project 128921); J.P.S.V. thanks CONACYT for a Ph.D. scholarship. P.M.H.K. thanks the University of Konstanz for financial support (Kr 04/75).

Notes and references

1 (*a*) E. Stadtman, *Science*, 1992, **257**, 1220; (*b*) F. R. Keene, *Coord. Chem. Rev.*, 1999, **187**, 121; (*c*) G. Yin, *Coord. Chem. Rev.*, 2010, **254**, 1826; (*d*) F. Hollmann, I. W. C. E. Arends, K. Buehler, A. Schallmey and B. Bühler, *Green Chem.*, 2011, **13**, 226; (*e*) S. P. de Visser, J. U. Rohde, Y.-M. Lee, J. Choc and W. Nam, *Coord. Chem. Rev.*, 2013, **257**, 381; (*f*) W. Nam, Y.-M. Lee and S. Fukuzumi, *Acc. Chem. Res.*, 2014, **47**, 1146.

2 (*a*) M. M. Whittaker and J. W. Whittaker, *Biophys. J.*, 1993, **64**, 762; (*b*) M. Mure, S. A. Mills and J. P. Klinman, *Biochemistry*, 2002, **41**, 9269; (*c*) P. Gamez, I. A. Koval and J. Reedijk, *Dalton Trans.*, 2004, 4079; (*d*) D. Holtmann, M. W. Fraaije, I. W. C. E. Arends, D. J. Opperman and F. Hollmann, *Chem. Commun.*, 2014, **50**, 13180.

3 (*a*) C. L. Hill, *Nature*, 1999, **401**, 436; (*b*) E. Roduner, W. Kaim, B. Sarkar, V. B. Urlacher, J. Pleiss, R. Gläser, W.-D. Einicke, G. A. Sprenger, U. Beifus, E. Klemm, C. Liebner, H. Hieronymus, S.-F. Hsu, B. Plietker and S. Laschat, *Chem. Cat. Chem.*, 2013, **5**, 82.

4 (*a*) R. A. Friesner, M. H. Baik, B. F. Gherman, V. Guallar, M. Wirstam, R. B. Murphy and S. J. Lippard, *Coord. Chem. Rev.*, 2003, **238–239**, 267; (*b*) P. E. M. Siegbahn and M. R. A. Blomberg, *Chem. Rev.*, 2010, **110**, 7040; (*c*) M. R. A. Blomberg, T. Borowski, F. Himo, R. Z. Liao and P. E. M. Siegbahn, *Chem. Rev.*, 2014, **114**, 3601; (*d*) S. P. de Visser, M. G. Quesne, B. Martin, P. Comba and U. Ryde, *Chem. Commun.*, 2014, **50**, 262; (*e*) A. Migliore, N. F. Polizzi, M. J. Therien and D. N. Beratan, *Chem. Rev.*, 2014, **114**, 3381.

5 (*a*) R. K. Wilson and S. Brooker, *Dalton Trans.*, 2013, **42**, 12075; (*b*) I. J. Hewitt, J.-K. Tang, N. T. Madhu, B. Pilawa, C. E. Anson, S. Brooker and A. K. Powell, *Dalton Trans.*, 2005, 429; (*c*) R. E. Norman, R. A. Leising, S. Yan and L. Que Jr., *Inorg. Chim. Acta*, 1998, **273**, 393.

6 (*a*) J. P. Saucedo-Vázquez, V. M. Ugalde-Saldívar, A. R. Toscano, P. M. H. Kroneck and M. E. Sosa-Torres, *Inorg. Chem.*, 2009, **48**, 1214; (*b*) V. M. Ugalde-Saldívar, M. E. Sosa-Torres, L. Ortiz-Frade, S. Bernès and H. Höpfl, *J. Chem. Soc., Dalton Trans.*, 2001, 3099; (*c*) V. M. Ugalde-Saldívar, M. E. Sosa-Torres and I. González, *Eur. J. Inorg. Chem.*, 2003, 978; (*d*) V. M. Ugalde-Saldívar, N. Farfán, A. R. Toscano, H. Höpfl and M. E. Sosa-Torres, *Inorg. Chim. Acta*, 2005, **358**, 3545; (*e*) J. P. Saucedo-Vázquez, *Reacciones de Deshidrogenación Oxidativa Promovidas por Hierro y Rutenio. Un Estudio Mecanístico*, *Tesis de doctorado*, Universidad Nacional Autónoma de México, 2012.

7 (*a*) V. Goedken and D. Busch, *J. Am. Chem. Soc.*, 1972, **94**, 7355; (*b*) C. J. Raleigh and A. E. Martell, *Inorg. Chem.*, 1985, **24**, 142; (*c*) W. R. Harris, I. Murase, J. H. Timmons and A. E. Martell, *Inorg. Chem.*, 1978, **17**, 889; (*d*) M. Goto, M. Takeshita, N. Kanda, T. Sakai and V. Goedken, *Inorg. Chem.*, 1985, **24**, 582; (*e*) M. Goto, N. Koga, Y. Ohse, Y. Kudoh, M. Kukihara, Y. Okuno and H. Kurosaki, *Inorg. Chem.*, 2004, **43**, 5120; (*f*) M. Goto, Y. Ohse, S. Koga, Y. Kudo, R. Kukihara and H. Kurosaki, *Bull. Chem. Soc. Jpn.*, 2004, **77**, 987.

8 (*a*) D. Wang, Y. Shiraishi and T. Hirai, *Chem. Commun.*, 2011, **47**, 2673; (*b*) Y. Shiraishi, K. Tanaka and T. Hirai, *Appl. Mater. Interfaces*, 2013, **5**, 3456.

9 (*a*) B. Zhu and R. J. Angelici, *Chem. Commun.*, 2007, 2157; (*b*) L. Aschwanden, T. Mallat, F. Krumeich and A. J. Baiker, *Mol. Catal. A: Chem.*, 2009, **309**, 57.

10 I. Murahashi, Y. Okano, H. Sato, T. Nakae and N. Komiya, *Synlett*, 2007, **11**, 1675.

11 A. P. Woodham, G. Meijer and A. Fielicke, *J. Am. Chem. Soc.*, 2013, **135**, 1727.

12 B. N. Zope, D. D. Hibbitts, M. Neurock and R. J. Davis, *Science*, 2010, **330**, 74.

13 (*a*) L. Que Jr. and W. B. Tolman, *Angew. Chem., Int. Ed.*, 2002, **41**, 1114; (*b*) B. F. Minaev, *Russ. Chem. Rev.*, 2007, **76**, 988; (*c*) J. P. Roth, *Curr. Opin. Chem. Biol.*, 2007, **11**, 1; (*d*) J. Cho, R. Sarangi and W. Nam, *Acc. Chem. Res.*, 2012, **45**, 1321.

14 J. P. Layfield and S. Hammes-Schiffer, *Chem. Rev.*, 2014, **114**, 3466.

15 (*a*) J. P. Collman, N. Devaraj, R. Decréau, Y. Yang, Y. Yan, W. Ebina, T. Eberspacher and C. Chidsey, *Science*, 2007, **315**, 1565; (*b*) L. Que and W. Tolman, *Nature*, 2008, **455**, 333; (*c*) B. Meunier, S. Visser and S. Shaik, *Chem. Rev.*, 2004, **104**, 3947; (*d*) D. Wang, K. Ray, M. J. Collins, E. R. Farquhar, J. R. Frisch, L. Gómez, T. A. Jackson, M. Kerscher, A. Waleska, P. Comba, M. Costas and L. Que, *Chem. Sci.*, 2013, **4**, 282.

16 D. Stanbury, O. Haas and H. Taube, *Inorg. Chem.*, 1980, **19**, 518.

17 D. Bhattacharya, S. Maji, K. Pal and S. Sarkar, *Inorg. Chem.*, 2008, **47**, 5036.

18 (*a*) Y. V. Geletii, C. L. Hill, R. H. Atalla and I. A. Weinstock, *J. Am. Chem. Soc.*, 2006, **128**, 17033; (*b*) O. Snir, Y. Wang, M. E. Tuckerman, Y. V. Geletii and I. A. Weinstock, *J. Am. Chem. Soc.*, 2010, **132**, 11678; (*c*) R. Neumann, *Inorg. Chem.*, 2010, **49**, 3594; (*d*) R. Neumann and M. Dahan, *Nature*, 1997, **388**, 353; (*e*) I. Efremenko and R. Neumann, *J. Am. Chem. Soc.*, 2012, **134**, 20669.

19 J. R. Perez, S. Banwart and I. Puigdomenech, *Appl. Geochem.*, 2005, **20**, 2003.

20 E. Bill, C. Haas, X. Ding, W. Maret, H. Winkler, A. X. Trautwein and M. Zeppezauer, *Eur. J. Biochem.*, 1989, **180**, 111.

21 (*a*) E. I. Solomon, T. C. Brunold, M. I. Davis, J. N. Kemsley, S.-K. Lee, N. Lehnert, F. Neese, A. J. Skulan, Y.-S. Yang and J. Zhou, *Chem. Rev.*, 2000, **100**, 235; (*b*) M. Costas, M. P. Mehn, M. P. Jensen and L. Que, *Chem. Rev.*, 2004, **104**, 939; (*c*) P. C. A. Bruijnincx, G. van Koten and R. J. M. Klein Gebbink, *Chem. Soc. Rev.*, 2008, **37**, 2716.

22 C. H. Langford and F. M. Chung, *J. Am. Chem. Soc.*, 1968, **90**, 4485.

23 J. Widegren and L. Bergström, *J. Eur. Ceram. Soc.*, 2000, **20**, 659–665.

24 H. Galster, *pH Measurement: Fundamentals, Methods, Applications, Instrumentations*, VCH, Weinheim, 1991.

25 R. G. Bates, *Determination of pH, Theory and Practice*, Wiley, New York, 1965.

26 A. I. Vogel, *Textbook of Quantitative Inorganic Analysis*, Longman, New York, 4th edn, 1978, p. 355.

27 H. J. Forman and I. Fridovich, *Arch. Biochem. Biophys.*, 1973, **158**, 396.

28 I. Rocchetta and H. Küpper, *New Phytol.*, 2009, **181**, 405.

29 (*a*) *N-Centered Radicals*, ed. Z. B. Alfassi, John Wiley & Sons, Chichester, 1998; (*b*) P. Chaudhuri and K. Wieghardt, *Prog. Inorg. Chem.*, 2001, **50**, 151.

30 T. Büttner, J. Geier, G. Frison, J. Harmer, C. Calle, A. Schweiger, J. Schönberg and H. Grützmacher, *Science*, 2005, **307**, 235.

31 D. L. J. Broere, B. de Bruin, J. N. H. Reek, M. Lutz, S. Dechert and J. I. van der Vlugt, *J. Am. Chem. Soc.*, 2014, **136**, 11574.

32 D. T. Sawyer, *Oxygen Chemistry*, Oxford University Press, New York, 1991.

33 (*a*) Y. Morimoto, J. Park, T. Suenobu, Y.-M. Lee, W. Nam and S. Fukuzumi, *Inorg. Chem.*, 2012, **51**, 10025; (*b*) J. Park, Y.-M. Lee, W. Nam and S. Fukuzumi, *J. Am. Chem. Soc.*, 2013, **135**, 5052.

34 A. R. Brash, *J. Biol. Chem.*, 1999, **274**, 23679.

35 (*a*) Y. Nishida and N. Tanaka, *J. Chem. Soc., Dalton Trans.*, 1994, 2805; (*b*) Y. Nishida, *Int. J. Chem.*, 2012, **4**, 1.

36 K. Zahir, J. H. Espenson and A. Bakac, *J. Am. Chem. Soc.*, 1988, **110**, 5059.

37 G. M. Yee and W. B. Tolman, *Met. Ions Life Sci.*, 2015, **15**, 131, DOI: 10.1007/978-3-319-12415-5_5.

38 T. I. Creaser, R. J. Geue, J. M. Harrowfield, A. J. Herlt, A. M. Sargeson, M. R. Snow and J. Springborg, *J. Am. Chem. Soc.*, 1982, **104**, 6016.